Supplementary Information

Post-seismic Deformation Mechanism of the July 2015 M_W 6.5 Pishan Earthquake Revealed by Sentinel-1A InSAR Observation

Sijia Wang [1*], Yongzhi Zhang[1,2*], Yipeng Wang[1], Jiashuang Jiao[1], Zongtong Ji[1], and Ming Han[1]

[1] College of Geology Engineering and Geomatics, Chang'an University, Xi'an 710054, China

[2] State Key Laboratory of Geo-information Engineering, Xi'an 710054, China

General information

Table S1. Details of co-seismic data were used in this study.

Orbit	Path	Acquisition	Frame	$B_{\perp}$(m)	Δt(days)	Inc. Angle(°)	Azi. Angle(°)
Ascending	056	20150630-20150724	120	-53	24	33.7	-169.3
Descending	136	20150624-20150718	465	26	24	41.4	-9.8
Descending	136	20150624-20150718	470	26	24	41.4	-9.8

Table S2. Source parameters of the 2015 Pishan earthquake.

Source	Lon. /(°)	Lat. /(°)	Strike /(°)	Dip /(°)	Length km	Width km	Slip m	M_W
USGS [a]	78.154	37.459	98	34	-	-	-	6.2
GCMT [b]	78.14	37.58	109	22	-	-	-	6.4
CENC [c]	78.1	37.5	115	23	-	-	-	6.5
Wen et al.	78.057	37.571	114	25	36	40	0.34	6.5
Uniform slip model	78.03 ±0.0004	37.50 ±0.0005	114.0 ±1.6	24 ±1.2	22.6 ±1.5	10.2 ±1.4	0.56 ±0.07	6.4
This study	78.03	37.50	114.0	25	36	40	0.35	6.5

[a] United States Geological Survey. [b] Global Centroid Moment Tensor Catalogue. [c] China Earthquake Network Center

Table S3. The Crust1.0 crustal layered earth structure

layer	Depth/ km	V_P/ km·s^{-1}	V_S/ km·s^{-1}	Rho(ρ) / kg·m^{-3}	η/ Pa·s
1	0.00	4.0000	2.1300	2370	∞
2	3.39	4.0000	2.1300	2370	∞
3	3.39	5.0000	2.8800	2540	∞
4	3.89	5.0000	2.8800	2540	∞
5	3.89	6.1000	3.5500	2740	∞
6	23.91	6.1000	3.5500	2740	∞
7	23.91	6.3000	3.6500	2780	1×10^{19}
8	41.65	6.3000	3.6500	2780	1×10^{19}
9	41.65	7.0000	3.9900	2950	1×10^{19}

Table S4. Details of post-seismic interferometric pairs were used in this study.

No.	Acquisition	B(km)	Δt(days)
1	20150928-20150718	-30.8650	72
2	20150928-20151209	93.5020	72
3	20150928-20160314	-81.1070	168
4	20151115-20150718	63.6750	120
5	20151115-20150928	-32.14	48
6	20151115-20151209	63.5330	24
7	20151115-20160126	-63.2924	72
8	20151115-20160219	-28.2582	96
9	20151115-20160314	-110.1997	120
10	20151115-20160805	42.3546	264
11	20160126-20150718	100.3620	192
12	20160126-20150928	34.0432	120
13	20160126-20151209	126.2527	48
14	20160126-20160219	34.5508	24
15	20160126-20160314	-47.4389	48
16	20160126-20160805	102.8146	192
17	20160219-20150718	70.2860	216
18	20160219-20150928	-8.2758	144
19	20160219-20151209	91.7461	72
20	20160219-20160314	-81.9811	24
21	20160219-20160805	69.4629	168
22	20160805-20151209	26.2252	240
23	20160805-20170508	-18.5854	276
24	20160922-20151209	99.8783	288
25	20160922-20160126	-26.6835	240
26	20160922-20160219	8.4833	216
27	20160922-20160314	-74.6694	192
28	20160922-20160805	76.4581	48

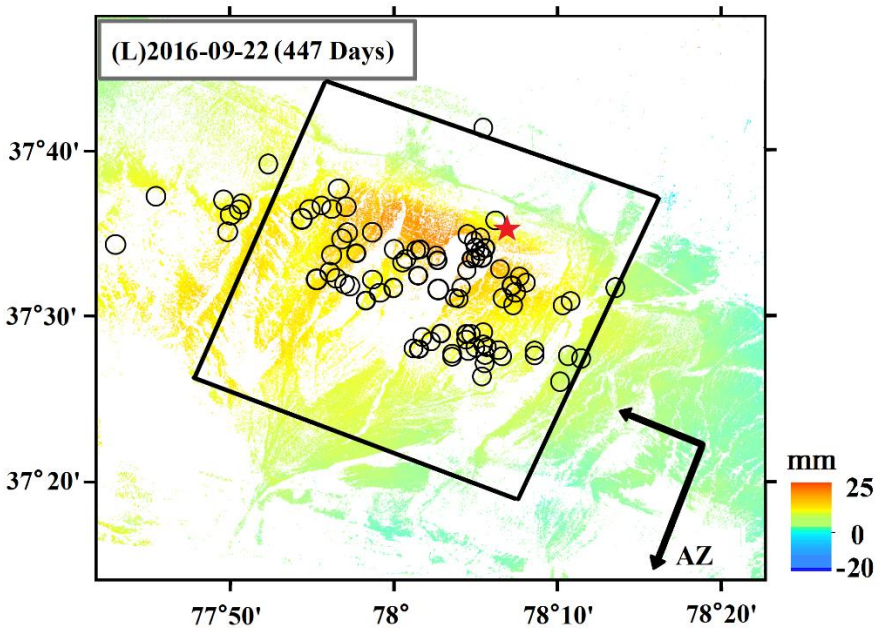

Figure S1. The cumulative LOS deformation from 15 November 2015 to 22 September 2016. Positive range change represents motion towards away from the satellite, while negative range change indicates motion away from the satellite. The red star represents the epicenter. The black circles indicate aftershocks (Mw≥3.0) up to 447 days after the mainshock. The black rectangle represents the surface projection of the modeled fault.

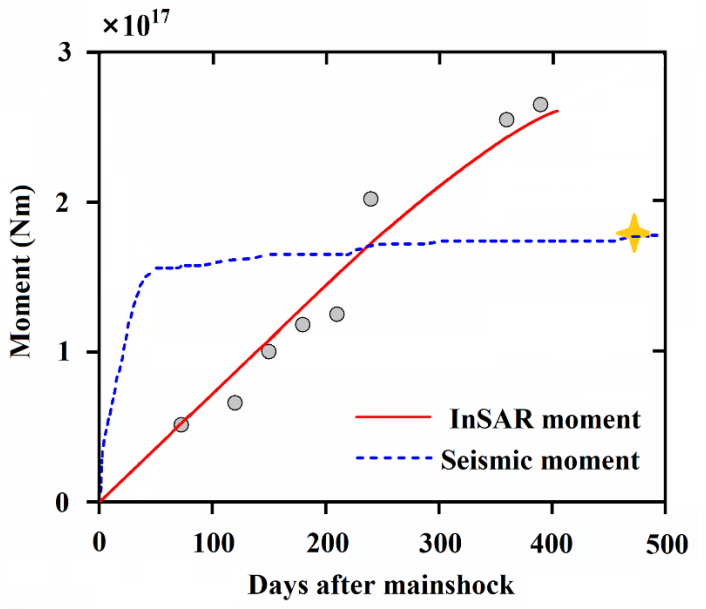

Figure S2. Time evolution of cumulative post-seismic moment released by afterslip (grey dots, with best-fitting exponential curve marked by the red line) and aftershocks (blue dashed line). The yellow star indicates the aftershock (Mw≥3.0) on October 5, 2016.

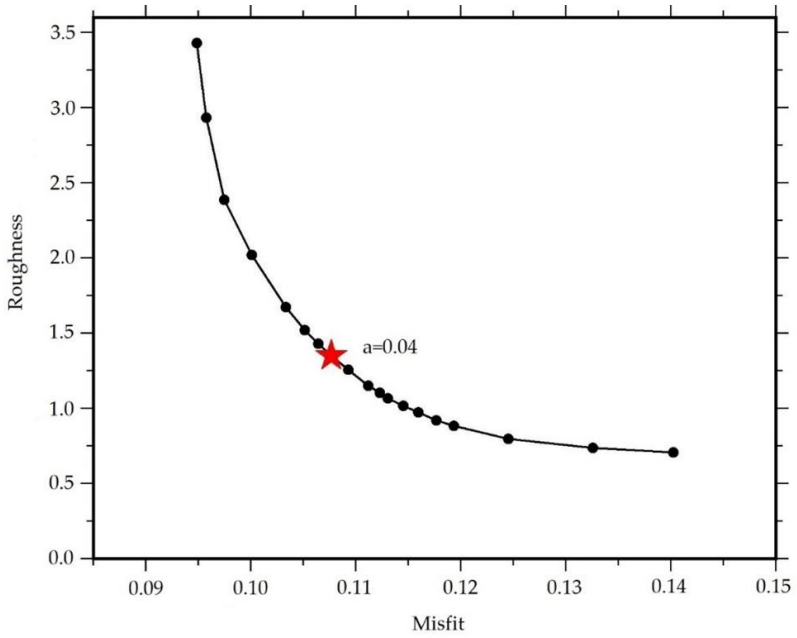

Figure S3. The curve representing the tradeoff between the model roughness and misfit. The red star indicates the location of the optimal smoothing parameter.

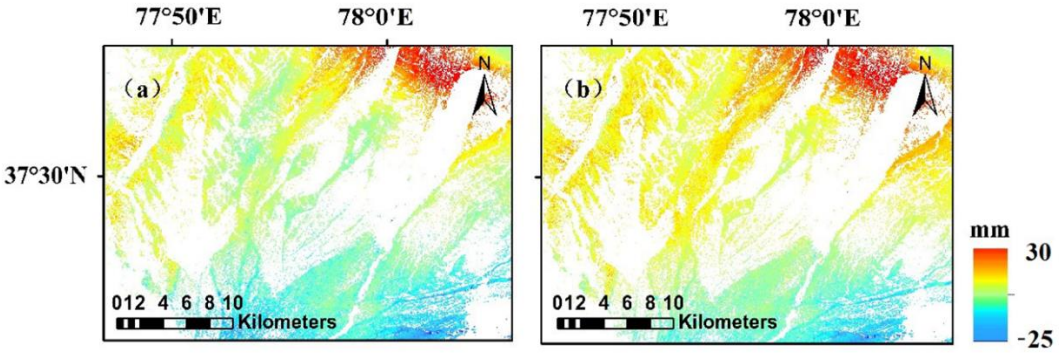

Figure S4. An example of atmospheric and orbital error correction for interferometry. (a) The uncorrected interference deformation image; (b) The image after atmosphere correction and orbit error correction.